

# Monitoring the Substrate-Induced Spin-State Distribution in a Cobalt(II)-Salen Complex by EPR and DFT

Giuseppina Magri,<sup>\*[a]</sup> Andrea Folli,<sup>[a]</sup> and Damien M. Murphy<sup>\*[a]</sup>

Ground state changes of (R,R')-N,N'-bis(3,5-di-tert-butylsalicylidene)-1,2-cyclohexane-diamino Co(II), following coordination of various pyridyl substrate has been examined by CW EPR, pulsed relaxation measurements and DFT. The solution-based Co(II) complex possesses a low spin (LS) state  $|yz, ^2A_2\rangle$  (with  $g$ -values of 1.96, 1.895, 3.14). Upon coordination of the pyridyl substrate, the resulting bound adduct reveals a distribution of LS 'base-on' species, possessing a  $|z^2, ^2A_1\rangle$  electronic ground state (with  $g$ -values of 2.008, 2.2145, 2.46) and a high spin (HS) species

(with  $g_{\text{eff}} = 4.6$ ). DFT indicated that the energy gap between the LS and HS state is dramatically lowered ( $\Delta E < 25 \text{ kJmol}^{-1}$ ) following substrate coordination. DFT suggests the main geometrical difference between the LS and HS systems is the severe puckering of the  $\text{N}_2\text{O}_2$  ligand backbone. The results revealed a tentative dependency on the  $\text{pKa-H}$  of the substrates for the spin distribution where, in most cases, the higher  $\text{pKa-H}$  substrate values favoured the HS species.

## Introduction

The study of spin crossover (SCO) compounds has attracted considerable attention among the scientific community over the past 30 years. In these compounds, transitions between the two spin states, namely the low spin (LS) or high spin (HS) states, can be facilitated by an external stimulus, such as temperature, pressure or irradiation which results in a shift of the spin-equilibrium. Recent examples demonstrating the broad range of potential applications for these SCO compounds include nanomaterials, molecular magnets and information storage devices.<sup>[1–6]</sup> The interest in these compounds has evidently not diminished since the early discovery of the spin transition effect by Cambi *et al.*<sup>[7]</sup> in 1931, with numerous review articles<sup>[8–10]</sup> published since then covering the theoretical and experimental behavior of such systems. For a long time, Fe(III) and Fe(II) systems dominated the SCO literature, with most of the Fe-based complexes possessing N- or O- donors<sup>[11–15]</sup> based on Schiff base ligands. These ligands, characterized by the general formula  $\text{R}_1\text{R}_2\text{C}=\text{NR}'$ , have therefore become a well-established framework for many SCO compounds, notably in Co(II) based systems.<sup>[16–22]</sup> Despite the growing interest in Co(II) based SCO systems, the literature remains dominated by Fe-based counterparts.<sup>[23,24]</sup> Nevertheless Co(II)-salen type complexes (bearing an  $\text{N}_2\text{O}_2$  ligand backbone) remain interesting systems to investigate, particularly as the SCO response can be induced by weak axial coordination of organic bases such as

pyridine.<sup>[25–31]</sup> In some cases, variations to the Salen ligand framework in these Co(II) complexes have also been observed to undergo thermally induced SCO in the solid-state.<sup>[32–34]</sup> On the other hand, substrate mediated SCO is arguably less well studied for such Co(II) systems. For example, computational studies have shown how 5-coordinate  $d^7$  Co(II)-salen type complexes bearing coordinated pyridine or imidazole as an axial substituent can produce a narrowing of the LS doublet ( $S=1/2$ ) and HS quartet ( $S=3/2$ ) energy gap, without the need for further external stimuli to induce the transition.<sup>[35]</sup> Indeed previous Electron Paramagnetic Resonance (EPR) studies have already shown how coordination of acetate from an acetic acid based solution in a Co(II)-salen type complex can lead to a change in spin state from LS Co(II) to HS Co(II).<sup>[36]</sup>

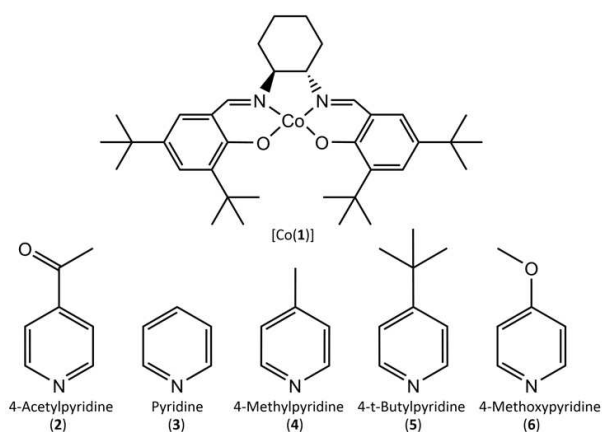
To date there has been limited studies regarding the nature of these substrate mediated SCO or spin distribution effects in Co(II) Schiff base complexes. One proposal for example, is that the event is driven through changes in the axial metal-ligand bond lengths, as observed in other nitrogen ligated Fe(II) complexes.<sup>[37–39]</sup> Another possibility is the coexistence or distribution of the two spin states at any given temperature, which arises from the small energy gap between the doublet and quartet states following coordination of the substrate.<sup>[40]</sup> Whilst the underpinning mechanism of this substrate induced spin distribution is not yet fully understood, the importance of the evolving research into this area cannot be underestimated in order to potentially help deliver a greater understanding of these spin distribution effects.

In this study, we therefore present our experimental and computational results into the substrate induced spin distribution in a Co(II)-salen complex ([Co(1)], Scheme 1) existing in both a low and high spin state. Continuous wave (CW) EPR reveals a distribution of both LS and HS Co(II) EPR signals, following the addition and coordination of various pyridyl based derivatives (Scheme 1) to the Co(II) complex under anaerobic conditions, as opposed to aerobic conditions. It is well documented how such 5-coordinate Co(II) complexes,

[a] G. Magri, Dr. A. Folli, Prof. D. M. Murphy  
School of Chemistry, Cardiff University  
Main Building, Park Place, Cardiff, CF10 3AT, UK  
E-mail: MagriG@cardiff.ac.uk  
MurphyDM@cardiff.ac.uk

Supporting information for this article is available on the WWW under <https://doi.org/10.1002/ejic.202101071>

© 2022 The Authors. European Journal of Inorganic Chemistry published by Wiley-VCH GmbH. This is an open access article under the terms of the Creative Commons Attribution License, which permits use, distribution and reproduction in any medium, provided the original work is properly cited.



**Scheme 1.** Structures of the [Co(1)] complex and the various pyridyl derivatives (2–6) used throughout this work.

bearing coordinated pyridine for example, can reversibly bind molecular oxygen forming a Co(III)-superoxo species under aerobic conditions.<sup>[41–43]</sup> In this work, the nature of the two coexisting spin states is investigated through CW EPR, pulsed EPR relaxation measurements ( $T_1$  and  $T_2$  experiments) and supplementary DFT computational data to broaden our understanding of this substrate mediated distribution of spin-states.

## Results and Discussion

### CW EPR of [Co(1)(X)] (X = 2–6) adducts under anaerobic conditions

The CW EPR spectrum of [Co(1)] recorded as a frozen solution in toluene is shown in Figure 1a. The spin Hamiltonian

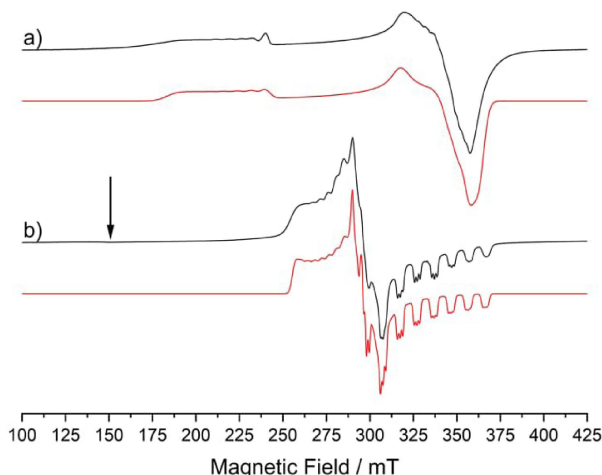


**Figure 1.** X-band CW EPR spectra (120 K) of a) [Co(1)] recorded in a toluene frozen solution, and b) after addition of 10 equiv. of (3) forming [Co(1)(X)]. The analogous EPR spectra of the remaining adducts [Co(1)(X)] are shown in the ESI. Arrow indicates field position of the second paramagnetic HS state. The simulated spectra are shown in the red trace.

parameters extracted by simulation of this experimental spectrum are listed in Table 1. The electronic structure of [Co(1)] and related salen-type derivatives have been explored extensively in the literature, and the reported EPR parameters (notably with  $g_z > g_{xy}$ ) have confirmed the  $|yz, ^2A_2\rangle$  ground state.<sup>[44,45]</sup> Upon coordination of an axial substrate, such as (2–6), the geometry is transformed to a square based pyramidal structure, as opposed to the former square planar arrangement for [Co(1)]. The ground state for these ligated [Co(1)(2–6)] adducts, is then altered to a  $|z^2, ^2A_1\rangle$ <sup>[36,40]</sup> LS state, as evident by the inversion of the  $g$ -tensor shown in Figure 1b for [Co(1)(3)]; the associated  $g$ -values are reported in Table 1. The simulations of all other [Co(1)(X)] adducts (see ESI) revealed the same inversion of the  $g$ -tensor, as reported in Table 1. DFT was also used to calculate the  $g$ -tensors (see ESI). The disparity between the DFT computed values and the experimentally determined  $g$ -tensor values (Table 1) is well documented in the literature for transition metals using hybrid functionals and arises from DFT not accurately reproducing the full spin-orbit coupling contribution to the  $g$ -values.<sup>[46]</sup> The superhyperfine interaction arising from the unpaired electron coupling to the  $^{14}\text{N}$  nucleus of the pyridyl bases (2–6) is well resolved in the EPR spectra (Figure 1b for [Co(1)(3)]; the spectra of the remaining adducts are shown in the ESI), which is expected due to the electronic ground state of the adduct and the  $\sigma$  donating ability of the N in the pyridine ring.<sup>[19]</sup> The  $^{14}\text{N}$  superhyperfine values extracted via simulation are listed in Table 2. These values are consistent with reported literature values for similar systems, and reveal an appreciable isotropic component to the  $^{14}\text{N}$  superhyperfine values.

The X-band EPR spectra of the adducts also reveals an unmistakable transition close to half-field, which is indicative of a HS state, and thus suggestive of co-existing HS and LS states in the system. The resulting low temperature EPR spectra, focusing on the half-field region (*ca.* 150 mT) for all five adducts [Co(1)(2–6)], are shown in Figure 2. At low temperatures (5 K), the LS Co(II) signal shown in Figure 1 is easily saturated and due to different relaxation times between these LS and HS

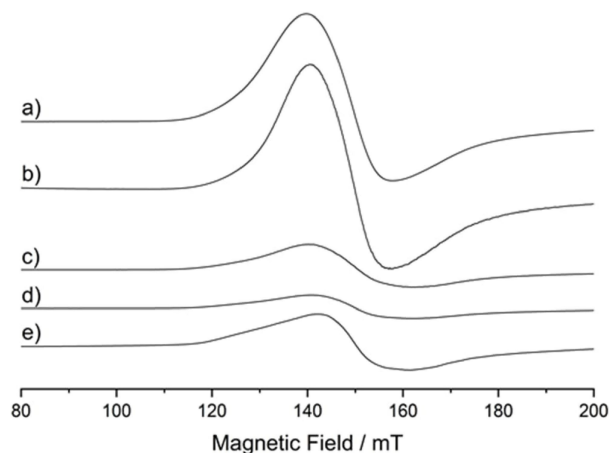


**Figure 2.** X-band CW EPR spectra (5 K) of the [Co(1)(X)] adducts, where the X-substrates corresponds to a) = (6), b) = (5), c) = (4), d) = (3) and e) = (2). All spectra were acquired under anaerobic conditions.

**Table 1.** Principal  $g$  and Cobalt hyperfine values of the [Co(1)] complex and associated [Co(1)(X)] adducts formed under anaerobic conditions.

Complex + adduct	$g_1$	$g_2$	$g_3$	$A_1$	$A_2$	$A_3$	Ref.
[Co(1)] <sup>[a]</sup>	1.96	1.91	3.14	160	−45	−340	t.w.
[Co(1)(2)] <sup>[b]</sup>	2.0137	2.215	2.465	±285	±30	±150	t.w.
[Co(1)(3)] <sup>[c]</sup>	1.98	2.215	2.33	±230	±60	±30	t.w.
[Co(1)(3)] <sup>[b]</sup>	2.008	2.2145	2.46	±282	±30	±138	t.w.
[Co(1)(4)] <sup>[b]</sup>	2.0137	2.2145	2.465	±277	±30	±138	t.w.
[Co(1)(5)] <sup>[b]</sup>	2.0135	2.214	2.46	±275	±30	±138	t.w.
[Co(1)(6)] <sup>[b]</sup>	2.0135	2.214	2.46	±277	±27	±138	t.w.
[Co(1)(NMI)] <sup>[b]</sup>	2.0195	2.22	2.43	±278	±45	±130	t.w.
[Co(1)] <sup>[a]</sup>	1.98	1.89	3.21	±125	<80	±400	[44]
[Co(salophen)] <sup>[d]</sup>	2.061	2.272	2.455	±300	±20	±10	[50]
[Co(1)(3)] <sup>[e]</sup>	2.01	2.20	2.46	±279	±40	±135	[42]
[Co(salen)(3)] <sup>[f]</sup>	2.006	2.212	2.45	+271	+33	+133	[51]
[Co(OEP)(3)] <sup>[g]</sup>	2.025	2.0326	2.326	±231	≤25	≤25	[43]
[Co(1)(HOAc)] <sup>[h]</sup>	2.02	2.28	2.42	±310	±120	±100	[36]
[Co(1)(3)] <sup>[i]</sup>	1.98	2.215	2.33	±230	±60	±30	[42]

[a] In toluene. [b] In a toluene solution with 10 equiv. of base, (NMI = 1-methylimidazole). [c] In a toluene solution of 45 equiv. of (3). [d] 1:1 mixture of DMF and MeOH under N<sub>2</sub>. [e] In a 10:1:5 mixture of toluene, acetic acid, and pyridine. [f] Single crystal. [g] In CHCl<sub>3</sub>. [h] In a toluene solution with 10 equiv. of HOAc. [i] In a 10:1:5 mixture of toluene, acetic acid, and pyridine. All hyperfine (A) values given in units of MHz.  $\alpha$ ,  $\beta$ ,  $\gamma$  = Euler angle rotation of the  $g$  and A frame with respect to the molecular frame. The  $g$ - and A-frame for [Co(1)] were simulated to be collinear using the values  $\alpha = 87^\circ$ ,  $\beta = 54^\circ$ ,  $\gamma = 97^\circ$ . For all [Co(1)(X)] adducts the  $g$ - and A-frame were simulated to be collinear using the values  $\alpha = 96^\circ$ ,  $\beta = 87^\circ$ ,  $\gamma = -170^\circ$ .

**Table 2.** Nitrogen principal hyperfine values obtained for the [Co(1)(X)] adducts.

Complex + adduct	$A_1^N$	$A_2^N$	$A_3^N$	Ref.
[Co(1)(2)] <sup>[a]</sup>	±38	±38	±45	t.w.
[Co(1)(3)] <sup>[a]</sup>	±38	±38	±45	t.w.
[Co(1)(3)] <sup>[b]</sup>	±38	±38	±45	t.w.
[Co(1)(4)] <sup>[a]</sup>	±38	±38	±45	t.w.
[Co(1)(5)] <sup>[a]</sup>	±37	±37	±45	t.w.
[Co(1)(6)] <sup>[a]</sup>	±38	±38	±45	t.w.
[Co(1)(NMI)] <sup>[a]</sup>	±45	±45	±52	t.w.
[Co(1)(3)] <sup>[c]</sup>	±40	–	–	[42]
[Co(salen)(3)] <sup>[d]</sup>	+40	–	–	[51]
[Co(OEP)(3)] <sup>[e]</sup>	+44	–	–	[43]
[Co(1)(3)] <sup>[f]</sup>	+40	–	–	[42]

[a] In a toluene solution with 10 equiv. of base, (NMI = 1-methylimidazole). [b] In a toluene solution with 45 equiv. of (3). [c] In a 10:1:5 mixture of toluene, acetic acid, and pyridine. [d] Single crystal. [e] In CHCl<sub>3</sub>. [f] In a 10:1:5 mixture of toluene, acetic acid, and pyridine. All hyperfine (A) values given in units of MHz.  $\alpha$ ,  $\beta$ ,  $\gamma$  = Euler angle rotation of the A-frame with respect to the molecular frame. For all [Co(1)(X)] adducts the A-frame was simulated using the values  $\alpha = 63^\circ$ ,  $\beta = 180^\circ$ ,  $\gamma = -107^\circ$ .

states, it is difficult to accurately quantify the relative contributions of both spin states at the same given temperature. Nevertheless, it is qualitatively clear from Figure 1 and Figure 2 that both spin states are present.

The HS signal shown in Figure 2 only appears when the coordinated substrate is present. Thus in order to understand whether the coordinated [Co(1)(X)] HS adducts were 5 or 6 coordinate (i.e., [Co(1)(X)<sub>*n*</sub>], where  $n=1$  or 2), a substrate titration experiment was performed, ranging in values of the added substrate (3) from 0.5 to 45 equivalents (Figure 3). At 0.5 equiv. of (3), an intense HS signal was already observed, with the LS signal being comprised of the coordinated [Co(1)(3)] adduct and the non-coordinated [Co(1)]. Between 1–5 equiv. of (3) the HS signal remains most intense and the absence of observable uncoordinated [Co(1)] under these conditions indicates that the 5-coordinated adduct is likely to be the most dominant species at this concentration. Upon

further additions of (3), between 10–45 equiv., the HS signal decreases in intensity and an additional LS signal begins to appear, which progressively increases in intensity up to 45 equiv. of (3). Simulation of this LS signal revealed the presence of a 6-coordinate adduct at this temperature. The deconvoluted simulation of the spectrum in Figure 3a (i.e., at the highest concentration of substrate) revealed a distribution of species, composed of 5-coordinate LS [Co(1)(3)<sub>*n=1*</sub>] and 6-coordinate LS [Co(1)(3)<sub>*n=2*</sub>] in 30:70 abundance ratio respectively (see ESI for deconvoluted spectra). This substrate titration experiment at 120 K, therefore suggests that the 5-coordinate [Co(1)(3)<sub>*n=1*</sub>] species appears most abundant and this can exhibit a distribution between LS and HS states, whereas the [Co(1)] and 6-coordinated adducts do not. It should also be noted that a temperature dependent equilibrium between the different coordination numbers 4, 5 and 6 ( $n=0-2$ ), likely exists and can inevitably alter the degree of coordination and spin state of the cobalt center, as indeed demonstrated in Ni(II) Schiff base complexes.<sup>[47–49]</sup> For example, Thies *et al.*<sup>[47]</sup> showed that within the temperature range 298–328 K, the association constants for binding a single pyridyl ligand to a Ni(II)-porphyrin forming a 5-coordinate complex and a second pyridyl ligand forming a 6-coordinated complex decreases as the temperature increases. As such, at lower temperatures, more substrate binding is expected, and this in turn will alter the amount of the HS versus the LS states, as revealed by the different EPR signals for the two states. In the current case, some of the EPR measurements were performed at 5 K, not only to enhance the amount of coordinated substrate, but also to overcome the fast-relaxation characteristics of the HS species, enhancing the intensity of this signal and hence the ease of characterisation. In summary it should be noted that temperature-dependent EPR studies were not conducted here, largely because we cannot accurately quantify the gradual transition between the HS and LS states based on the relative intensities of the EPR signals, but also because temperature effects will also influence the degree

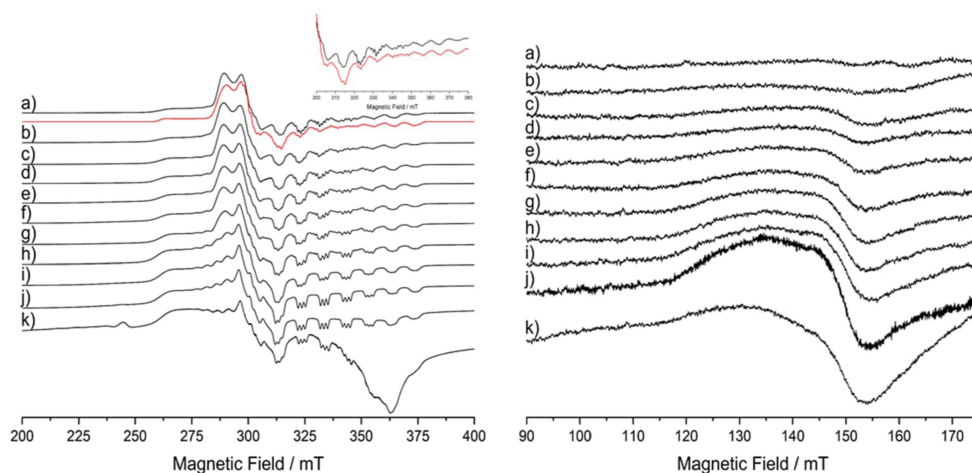


**Figure 3.** X-band CW-EPR spectra (120 K), recorded with 5 G modulation amplitude and 100 kHz field modulation of [Co(1)] containing a) 45, b) 40, c) 35, d) 30, e) 25, f) 20, g) 15, h) 10, i) 5, j) 1 and k) 0.5 equivalents of (3), showing the LS signals. Red trace indicates simulated data of a), where the signal is comprised of a mixture of [Co(1)(3)<sub>2</sub>] (~70%) and [Co(1)(3)] (~30%): the deconvoluted simulation is shown in the ESI. All EPR parameters are given in Table 1.

of substrate binding. Therefore extracting the temperature dependent contribution to SCO versus temperature dependent substrate binding effects is difficult to separate.

#### Computational DFT studies on the LS and HS Co(II) states

Natural bonding orbitals (NBO's) were calculated for the uncoordinated and coordinated Co(II) adducts in the LS state ( $S=1/2$ ). NBO analysis identified the electronic ground states for both [Co(1)] and the associated [Co(1)(X)] adducts, in agreement with the spectroscopic findings. The electronic ground state, predicted by DFT, for all five adducts reveals a  $d_z^2$  configuration in all cases. This DFT predicted electronic ground state are not only in good agreement with our spectroscopic findings (by evaluation of the  $g$ -tensor; see ESI), but also match other electronic ground state predictions for other 5-coordinated Co(salen) adducts obtained from DFT.<sup>[36,52]</sup> These are shown in Figure 4 for [Co(1)] and the [Co(1)(3)] adduct (the remaining adducts are shown in the ESI).

The optimised geometry calculated from DFT of the LS [Co(1)] complex shows a good agreement with experimental crystal structures of similar Co(salen) complexes obtained from X-ray data.<sup>[53]</sup> Specifically, the optimised geometry of LS [Co(1)] exhibits minor deviations of 0.02, 0.015, 0.004 and 0.008 Å in the Co–O<sub>1,2</sub> and Co–N<sub>1,2</sub> in-plane bond lengths respectively (atom numbering notation found in ESI), with the stereochemistry of the Co atom being square planar.<sup>[53]</sup> Our computational approach was adopted here in order to monitor the energy gap between the LS and HS states, in addition to the atomic charges of the Co atom, the Co–N&Co–O in-plane bond elongation and the Co–N<sub>3</sub> (pyridyl) bond lengths, enabling the characterization of key structural details between the LS and HS [Co(1)(X)] adducts. The LS–HS geometrical parameters are presented in Table 3, whilst the energy gap and atomic charges on the Co atoms are listed in Table 4.

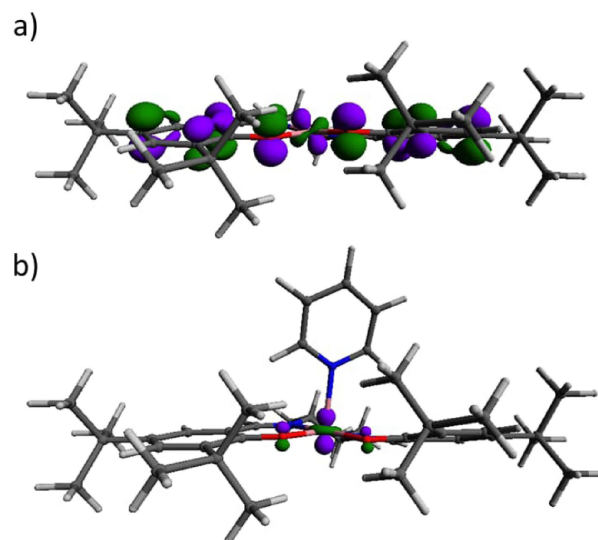


**Figure 4.** DFT computed orbital ground states for the SOMO of the low spin a) [Co(1)] ( $d_{z^2}$ ) complex and b) the [Co(1)(3)] adduct with axial coordination of (3) ( $d_{z^2}$ ).

Most notably, a marked structural difference can be observed between the LS and HS states in the [Co(1)(X)] adducts. This is most readily illustrated for the two spin states in [Co(1)(3)]. As shown in Figure 5, the ground state geometries for this adduct in the doublet (LS) and quartet (HS) spin states differ, most notably in the configuration adopted by the salen backbone. Specifically, the salen ligand in the LS state adopts a more planar arrangement, whereas the arrangement is distinctly puckered in the HS configuration. The computed LS [Co(1)(X)] geometries can be likened to the crystal structure of a LS [Co(salen)(3)] complex, where the Co–N<sub>3</sub> bond lengths differ by 0.133 Å when compared to our optimised [Co(1)(3)] geometry (Table 3). The depression angle  $\theta^\circ$  (N<sub>3</sub>–Co–N<sub>1</sub>) in the LS case are also comparable, resulting in a square pyramidal

**Table 3.** DFT computed geometrical parameters of [Co(1)] and the [Co(1)(X)] adducts.

Co-adduct	Co–N <sub>3</sub> length LS / Å	Co–N <sub>3</sub> length HS / Å	θ° (N <sub>3</sub> –Co–N <sub>1</sub> ) / HS	Co–N,O elongation HS / Å
[Co(1)]	N/A	N/A	N/A	N <sub>1,2</sub> =0.15, O <sub>1,2</sub> =0.06
[Co(1)(2)]	2.25	2.15	107.0	N <sub>1</sub> =0.21, N <sub>2</sub> =0.14, O <sub>1</sub> =0.05, O <sub>2</sub> =0.06
[Co(1)(3)]	2.23	2.15	107.0	N <sub>1</sub> =0.22, N <sub>2</sub> =0.14, O <sub>1</sub> =0.05, O <sub>2</sub> =0.06
[Co(1)(4)]	2.23	2.15	108.1	N <sub>1</sub> =0.23, N <sub>2</sub> =0.13, O <sub>1</sub> =0.06, O <sub>2</sub> =0.07
[Co(1)(5)]	2.24	2.16	110.2	N <sub>1</sub> =0.19, N <sub>2</sub> =0.14, O <sub>1</sub> =0.06, O <sub>2</sub> =0.06
[Co(1)(6)]	2.23	2.14	107.6	N <sub>1</sub> =0.22, N <sub>2</sub> =0.14, O <sub>1,2</sub> =0.06
[Co(1)(NMI)]	2.20	2.13	108	N <sub>1</sub> =0.22, N <sub>2</sub> =0.14, O <sub>1</sub> =0.06, O <sub>2</sub> =0.05

**Table 4.** DFT computed electronic parameters of [Co(1)] and the resulting [Co(1)(X)] adducts.

Co-adduct	pKa–H of base (3-6)	ΔE (LS-HS) / kJ mol <sup>-1</sup>	Atomic Charge Co (LS)	Atomic Charge Co (HS)
[Co(1)]	N/A	37.14	0.732	1.131
[Co(1)(2)]	3.59	19.48	0.702	1.036
[Co(1)(3)]	5.20	18.72	0.695	1.036
[Co(1)(4)]	5.98	18.21	0.696	1.035
[Co(1)(5)]	5.99	17.71	0.699	1.040
[Co(1)(6)]	6.95	17.51	0.696	1.035

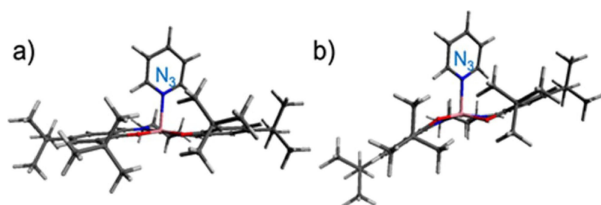


**Figure 5.** DFT optimised geometry of a) LS [Co(1)(3)] and b) HS [Co(1)(3)], noting the atom numbering of N<sub>3</sub>.

structure as evidenced by our DFT results.<sup>[54]</sup> From our DFT calculations, it is also clear that a shortening of the axial Co–N<sub>3</sub> bond length occurs in the HS state (Table 3) with the Co(II) center raised out of the N<sub>2</sub>O<sub>2</sub> framework. When the adduct exists in the HS state, an elongation of both the Co–O<sub>1,2</sub> and Co–N<sub>1,2</sub> in plane donor bond lengths is observed, although this elongation is more pronounced for the Co–N bonds compared to the Co–O bonds. This causes a slight puckering of the N<sub>2</sub>O<sub>2</sub>

backbone in the HS state (see ESI). There is no literature data on the crystal structures of HS [Co(salen)(pyridyl)] systems. However the crystal structure of a HS [Co(saloph)(2-methylimidazole)] was reported,<sup>[26]</sup> where the Co atom was lifted out of the saloph ligand plane resulting in a depression angle θ° of 108.6°, a discrepancy of only 0.6° (compared to our DFT optimised geometry of [Co(1)(NMI)] in Table 3). Moreover, their Co–N<sub>3</sub> bond length only differed from our DFT findings by 0.057 Å. Taken collectively, our molecular modelling shows a good agreement in our LS and HS [Co(1)(X)] geometries with available experimental observation.

As stated above, the presence of the axial ligand lifts the Co(II) centre out of the plane, causing the Co–N<sub>1</sub> and Co–N<sub>2</sub> in-plane bonds to elongate by different magnitudes (Figure 5b). Elongation of the in-plane Co–N and Co–O bonds are indicative of a weaker interaction between the Co(II) centre and the N<sub>2</sub>O<sub>2</sub> backbone.<sup>[55]</sup>

This is further exemplified by an increase in Co atomic charges in all ligated species upon transition from LS to HS (Table 4). The Co–N<sub>3</sub> bond shortens by 0.08–0.1 Å upon transitioning from LS to HS, reflective of tighter pyridyl association in the HS state and this can be ascribed to the increased interaction between the d<sub>z</sub><sup>2</sup> orbital (Figure 4) and the bound axial pyridyl substrates. In a framework, where the pyridyl adduct is a major contributor to the charge on the central Co atom, one would expect tighter association (shorter Co–N<sub>3</sub> bond) in the HS state to lead to a net lowering of the Co atomic charge relative to the LS state. However, this is not observed (Table 4), suggesting the elongation of the N<sub>2</sub>O<sub>2</sub> backbone and subsequent weakening of the in-plane Co–N and Co–O bonds dictates the change in charge on the Co atom more so than the bound pyridyl.

#### Pulsed EPR relaxation measurements of [Co(1)(2, 5, 6)]

The choice of pyridyl derivatives selected in this work (2–6) was intended to explore the role of substrate pKa–H on the relative LS-HS distribution of observed spin states. The double integrals (D.I.) of the HS EPR signal recorded at 5 K (Figure 2 and *vide infra*) indeed show a strong correlation between the pKa–H values of the substrate and the corresponding intensity of the HS signal, with substrates (6), (5) and (2) generating the strongest signals. As (2) has the lowest pKa–H among those selected substrates, it was important to ensure that the intensity of the HS signals was in fact due to a difference in concentration or abundance between the HS forms of the adducts rather than originating from differences in spin relaxation. Therefore, T<sub>1</sub> and T<sub>2</sub> measurements were performed at the same field position (B = 178.3 mT) for all three adducts. At this low field position, only the HS species contributes to the relaxation measurements.

From Figure 6 it is clear that the signal to noise ratio (S/N) is significantly worse for [Co(1)(2)] compared to the (5) and (6) based adducts. This is likely due to the lower abundance of the HS species in [Co(1)(2)] producing a weaker echo response. From analysis of the T<sub>2</sub> values extracted for these three specific

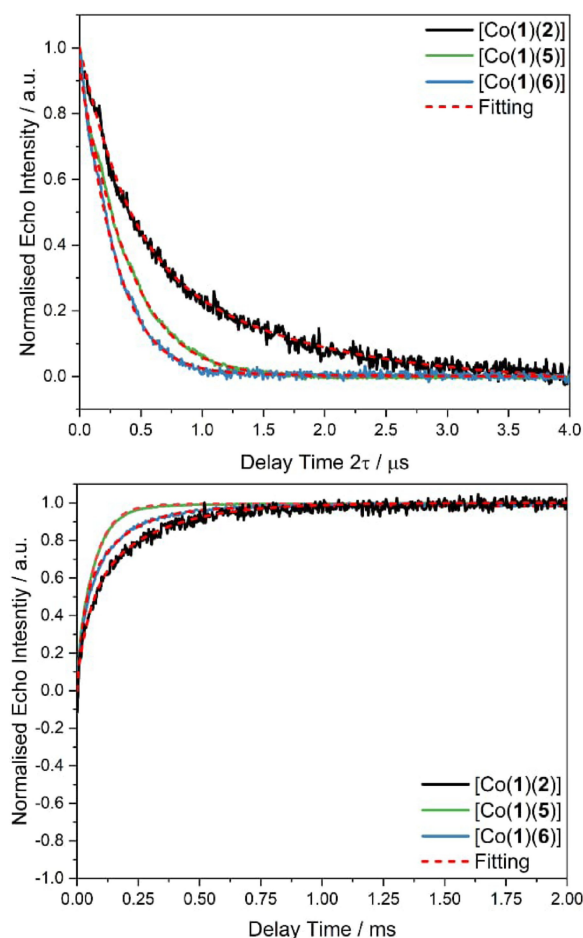


**Figure 6.** Two-pulse Hahn-echo decay measured at 5 K (top) and Echo-detected inversion recovery (bottom) for the [Co(1)] adducts with 10 equiv. of (6), (5) and (2) shown in the blue, green and black trace respectively. The fitted data is shown in the red dashed trace.

adducts, it is evident that the  $T_2$  relaxation times for [Co(1)(5)] and [Co(1)(6)] are very similar to each other, and significantly shorter relative to [Co(1)(2)]. Interestingly, [Co(1)(2)] produces the longest  $T_2$  value but the least intense HS signal in the CW EPR spectrum between these three bases (Figure 2). If relaxation was a dominant contributory factor influencing the D.I.s of the CW EPR spectra, one would expect the [Co(1)(2)] adduct to produce the most intense HS signal, with [Co(1)(6)] bearing the weakest HS signal. As this is not the case, it implies that  $T_2$  relaxation does not influence the intensity of the HS signal.

The  $T_1$  data shows a similar trend to the  $T_2$  values (Figure 5). The  $T_1$  time for [Co(1)(2)] is approximately double that of the other two adducts (Table 5), even though this [Co(1)(2)] adduct produced the smallest D.I. Comparative spin-spin and spin-

Co-adduct	pKa-H	$T_1$ / ms	$T_2$ / $\mu$ s
[Co(1)(2)]	3.59	$0.1202 \pm 0.0037$	$0.7048 \pm 0.00715$
[Co(1)(5)]	5.99	$0.0559 \pm 0.0011$	$0.3693 \pm 0.00245$
[Co(1)(6)]	6.95	$0.0749 \pm 0.0021$	$0.2933 \pm 0.0036$

lattice relaxation times for related HS Co(II) complexes are scarce in the literature, as these are system, temperature, field and  $\tau$  dependant parameters making direct comparisons difficult. However, HS Co(II) complexes typically have very fast relaxation times (especially  $T_1$ ) due to zero-field splitting ( $S > 1/2$ ), and hence the better resolved EPR spectra are usually obtained at low temperatures. A HS Co(DTPA) complex was found to have a reported  $T_1$  value of 1.6 ms at 6.5 K whereas at 8.2 K it was 25  $\mu$ s, showing the strong temperature dependency upon the relaxation values.<sup>[56]</sup> Although it has been suggested in the literature that differences in  $T_1/T_2$  relaxation times for Co(II) complexes bearing coordinated bases may be influenced by different molecular weights or bulk of the axial substrates,<sup>[57]</sup> we have no evidence to indicate that such an effect occurs in the [Co(1)(X)] system. Indeed the variation in signal intensities observed for the HS states (as shown in Figure 2), appears to be due to differences in relative abundances of these HS adducts, rather than wide variation in relaxation times.

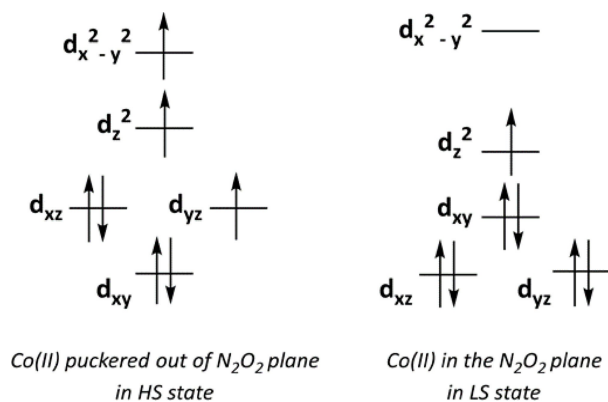
### The nature of the co-existing Co(II) spin states

The EPR spectra of the [Co(1)(X)] adducts recorded at 120 K and 5 K (Figure 1 and Figure 2), revealed the presence of two different spin states for the Co(II) adducts. This observation is additionally supported by published magnetic susceptibility measurements by Marzilli and Marzilli,<sup>[58]</sup> on a Co(II)-saloph complex (where saloph = N, N'-bis (salicylidene)-o-phenylene-diamino), bearing coordinated pyridine and 1-methylimidazole substrates. They showed differing magnetic moments of ca. 2  $\mu_B$  and 4–5  $\mu_B$  for the LS and HS states respectively. The observed temperature dependency was also explained as arising from an equilibria between the LS and HS states.<sup>[58]</sup> Furthermore, reported computation of the crystal cell of a related [Co-salen(3)] adduct revealed the existence of two unique molecular units per cell, which were assigned to the LS and HS forms of the adduct.<sup>[35]</sup> Both of these studies<sup>[35,58]</sup> therefore confirms the co-existence of two different Co(II) spin states that may form in the presence of coordinated pyridyl based substrates (2–6).

In the current study, two different geometries are adopted for the two different spin-states. From the DFT results, the main structural difference between the LS and HS states is the puckering of the ligand backbone and a raising of Co(II) out of the  $N_2O_2$  plane in the HS state (Figure 5). This geometric perturbation in the HS state leads to a modified square-pyramidal  $d$ -orbital energy diagram (Scheme 2).

The alteration of the  $d$ -orbitals is synonymous with a further decrease in symmetry from the LS to HS state. The  $d$ -orbital splitting in Scheme 2 indicates a higher degree of  $\sigma$  and  $\pi$  donating ability from the axial substrate, which is reflected in a shorter Co–N<sub>3</sub> bond and a puckering of the  $N_2O_2$  ligand backbone in the HS state (Figure 5 and Table 3).<sup>[59]</sup>

A similar lowering of the Co(II)  $d_{x^2-y^2}$  orbital, facilitating access to the HS state, was also observed in proton-mediated SCO of a cobalt heme analogue (Co-TPP) (where TPP = tetraphenylporphyrin) as reported by Zhao *et al.*<sup>[22]</sup> In their



**Scheme 2.** Simplified model of Co(II) d-orbital splitting for a square-base pyramid where left: Co(II) out of plane HS d7 and right: within the plane LS  $d^7$ . Scheme adapted from Jurca *et al.*<sup>2</sup>

study, 2-methylimidazole was axially coordinated to the Co(II) heme structure promoting the LS Co(II) state. However, upon removal of the proton from the N<sub>2</sub> position in the 2-methylimidazole substrate (pK<sub>a</sub>-H = 7.86), a HS Co(II) state was observed. This was ascribed to the neutral ligated imidazole having a small metal out-of-plane displacement indicative of the LS Co(II) species, whereas in the deprotonated state, the large out-of-plane displacements of the central metal was characteristic of a HS complex with the  $d_{x^2-y^2}$  orbital having sufficiently lower energy. When both neutral hindered and non-hindered imidazole's (e.g. 1-methylimidazole/**NMI**, pK<sub>a</sub>-H = 7.4) were coordinated, all complexes were observed to be LS.

In the current work, we have found that axial coordination of a neutral non-hindered imidazole substrate such as (**NMI**) (see ESI) to [Co(1)], results in the co-existence of two spin-states, producing the same HS EPR signal analogous to the pyridyl derivatives (Figure 2). In this case, DFT confirms that the Co(II) centre is once again lifted out of the plane (puckered) in the HS state (see ESI). To access this HS state, the in-plane donor bonds must elongate such that the short metal-N<sub>3</sub> bond can lift the metal centre out the plane. The DFT computed Co-N<sub>1,2</sub> bond lengths (2.13 and 2.04 Å) in the HS [Co(1)(**NMI**)] adduct agree with the average distances between the metal and porphyrin nitrogen atoms in the HS [Co(TPP)(2Melm<sup>-</sup>)]<sup>-</sup> complex (2.079 Å).<sup>[22]</sup> In the case of [Co(TPP)(**NMI**)]<sup>[60]</sup> only the LS state was observed, as the (**NMI**) was regarded as too weak to raise the Co(II) out of the porphyrin plane. Subsequently, the  $d_{x^2-y^2}$  orbital was insufficiently lowered in energy preventing access to the HS state (Scheme 2). This indicates that the strength of the axial substrate interaction, in addition to the ability of the in-plane donor bonds to elongate, will influence the ability to access the HS state. The fact that the HS state can be achieved with [Co(1)(**NMI**)] possessing a salen N<sub>2</sub>O<sub>2</sub> backbone, may reflect the rigidity of the porphyrin backbone when coordinated to (**NMI**), prohibiting the elongation of the N<sub>4</sub> bonds.

The strength of the metal-axial substrate bond can be gauged from the pK<sub>a</sub>-H of the axial N donor species as outlined by Kennedy *et al.*<sup>[26]</sup> Through magnetic susceptibility measurements conducted on a Co(II)-salen/saloph complex bearing a

coordinated substrate at room temperature, the authors showed that the higher the pK<sub>a</sub>-H of the axial substrate (pyridyl or imidazole derivatives), the higher the  $\mu_{\text{eff}}$ . This resulted in a decrease in the LS-HS energy separation, suggesting a higher distribution of HS species will occur upon increasing the pK<sub>a</sub>-H of the substrate. As evident from Figure 2, the most intense HS signal indeed arises for the [Co(1)(6)] adduct where the pyridyl substrate has the highest pK<sub>a</sub>-H value (of 6.95).

### Influence of substrate pK<sub>a</sub>-H values

According to Neese *et al.*,<sup>[61]</sup> the energy gap required for a complex to undergo spin crossover behaviour lies in the range of 0–25 kJ mol<sup>-1</sup>. The non-coordinated [Co(1)] complex, as expected, falls outside of this range (37.14 kJ mol<sup>-1</sup>) hence the observation of only the CW EPR signal assigned to the LS state (Figure 1a). By comparison, in all the coordinated adducts studied here, the energy gap between the LS and HS states is dramatically lowered, falling into the spin crossover range. The same trend was observed in quantum chemical calculations of a Co(II)-salen complex bearing pyridine and imidazole ligands, which concluded that such systems are perhaps suitable for spin crossover events.<sup>[35]</sup>

The energy gaps reported in the current work supports the presence of a high spin Co(II) EPR signal observed at both liquid nitrogen (120 K) and liquid helium temperatures (5 K). Kennedy *et al.*<sup>[62,26]</sup> have previously considered the influence of substrate pK<sub>a</sub>-H on the LS-HS energy gaps in Co-salen and Co-salophen adducts. Considering the chemically and structurally related bases, similar relationships were observed in this work (eg., the relative pK<sub>a</sub>-H of the bases varies in the order of (3) < (4) < (5) < (6), which in turn translates into a narrowing of the energy gap upon increasing the pK<sub>a</sub>-H). The same trend was observed for the (**NMI**) compared to an imidazole adduct. This is clear in Figure 2 where substrate (6), with a pK<sub>a</sub>-H value of 6.47, was seen to have the most intense HS signal (alongside the lowest energy gap), whereas (3), with a pK<sub>a</sub>-H value of 5.2, had the lowest HS signal intensity (alongside the highest energy gap out of these 4 bases), as evident in Figure 7.

Recognising that pK<sub>a</sub> is a measure of the  $\sigma$  donating ability of the base, the better  $\sigma$  donors give rise to a stronger interaction between the Co(II)  $d_z^2$  orbital and the axial pyridyl base N donor leading to a greater stabilisation of the HS state. A depression angle ( $\theta^\circ$ , N<sub>3</sub>-Co-N<sub>1</sub>) greater than 102° is associated with a larger decrease in the energy gap between LS and HS states in [Co(II)(salen)L] and [Co(II)(saloph)L], where L = imidazole or pyridyl derivatives.<sup>[26]</sup> From the optimised geometries of the HS complexes, for all pyridyl coordinated adducts, the depression angle exceeds 102° and this suggests that there is a greater stabilisation of the HS state. This, in turn, helps to provide a further explanation for the occurrence of a HS signal in the CW EPR spectra.

The choice of pyridyl derivatives used in this study (Scheme 1) was further elaborated in order to explore any alterations to the HS-LS signals following a change not only in pK<sub>a</sub>-H, but also in terms of the variability in potential inductive

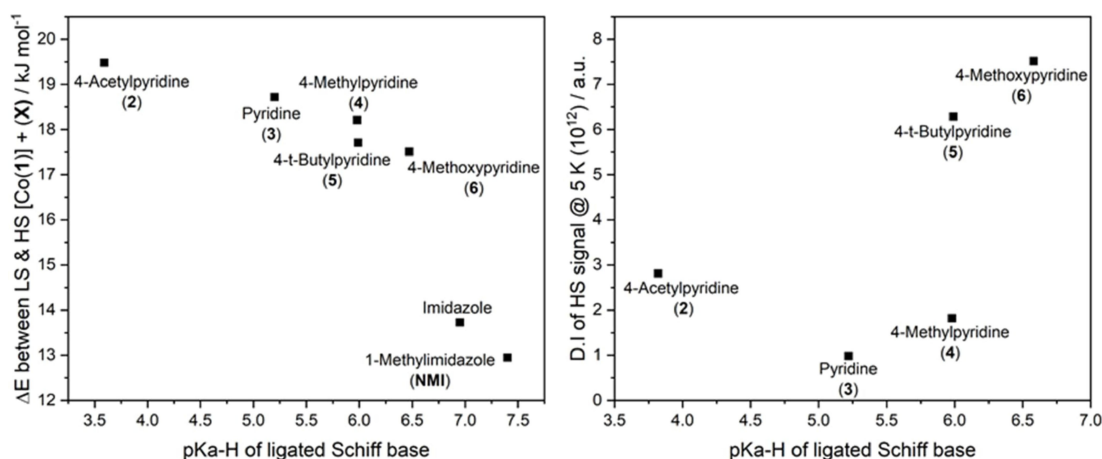


**Figure 7.** Doublet-Quartet energy gap for [Co(1)(2–6)] complexes as a function of pKa–H of Schiff base, calculated with B3LYP 6-311 + G(2d,p) on all atoms except Co where def2-TVZPP was used (left); Double Integral (D.I.) of HS [Co(1)(2–6)] signals acquired at 5 K as a function of pKa–H of Schiff base (right).

effects promoted by the substituents –CH<sub>3</sub> and *t*-butyl groups. The atomic charges on the central Co atom were presented in Table 4.

The inductive effect of a substituent at the 4-position, through the pyridine  $\pi$ -system, would result in a lower Co atomic charge within both spin-states. For example, an acetyl group, as in (3) is electron withdrawing, thus one would expect the charge of the Co centre in [Co(1)(3)] to be more positive, compared to electron donating groups such as a methyl in [Co(1)(4)] or (5) and the methoxy group in [Co(1)(6)]. Although a narrowing of LS–HS energy gap is observed upon increasing pKa–H of the pyridyl species (Table 4 and Figure 7), the increased basicity from (2)–(6) is not reflected in the atomic charge of the Co,

The DFT results indicate that the [Co(1)(6)] adduct had the lowest  $\Delta E$  (LS–HS) gap (along with highest pKa–H) while the [Co(1)(5)] adduct has the second lowest  $\Delta E$  gap, (along with the second highest pKa–H); see Figure 7. In contrast, [Co(1)(2)] has the largest  $\Delta E$  gap, but lowest pKa–H value, along with a considerable signal intensity (Figure 2). Therefore, pyridyl ligand sterics (bulkiness of the 4-position) also appear to influence the population and distribution of the HS state alongside the pKa–H value. This is also observed in our previous work using weak organic acids such as benzoic, propanoic and acetic acid.<sup>[36]</sup> It must be noted that the overall concentrations of samples and quality of ‘glass’ when freezing samples were kept as consistent as possible to rule out any changes in the HS signal intensity to be as a result of these two factors.

## Conclusion

In this work, the observation of a LS–HS distribution upon coordination of a pyridyl base substrate to [Co(1)] has been monitored using EPR and DFT, revealing the co-existence of both Co(II) spin states. The experiments also suggest that the adducts in frozen solution responsible for the HS states were all

5-coordinate. By varying the pKa–H of the coordinating pyridyl base substrate, the intensity of the EPR signal for the HS state was found to favour the more  $\sigma$  donating substrates and higher pKa–H values. Pulsed relaxation data on a selection of the adducts revealed that the observed changes in the relative EPR signal intensity of the HS state was not due to differences in the  $T_1$  and  $T_2$  relaxation times, but rather must arise from difference in the chemical properties of the substrate itself. The conclusions based on the molecular DFT modelling match the experimental findings, whereby the lowering of the HS energy state is directly correlated with a weakening in the Co–N,O in-plane bonds upon coordination of the axial pyridyl base. Strong axial coordination of the substrate distorts the N<sub>2</sub>O<sub>2</sub> salen backbone, lifting Co(II) out of the plane, and thereby stabilising the HS state making it accessible. Moreover, the narrowing of  $\Delta E$  gap between the LS and HS states may also be attributed to an increase in pKa–H of the pyridyl base. This work has therefore shown how the subtle differences in the nature of the substrate can ultimately and synergistically determine the distribution of the LS and HS states in these Co(II) complexes.

## Experimental Section

### Sample Preparation

[Co(1)] was obtained from Sigma-Aldrich (CAS: 176763-62-5). For acquisition of the CW and pulse EPR spectra, 20 mM aliquots of this [Co(1)] complex dissolved in toluene was used resulting in a deep orange/red coloured solution. Stock solutions of commercially available pyridyl analogues (all ex Sigma-Aldrich), including 4-acetylpyridine (2), pyridine (3), 4-methylpyridine (4), 4-*t*-butylpyridine (5), and 4-methoxypyridine (6) were prepared in the same solvent system whereby a 1  $\mu$ L aliquot was equivalent to 10 equiv. of the base and was added directly to the 20 mM solution of [Co(1)] under air. The experiments conducted with 1-methylimidazole (NMI) were performed the same way. The solution immediately changed colour to dark brown indicating coordination of the substrate. The sample was then thoroughly degassed, using a

Young EPR tube attached to a Schlenk line operating under a N<sub>2</sub> atmosphere and following repeated freeze pump thaw cycles to remove any traces of molecular oxygen.

## EPR Measurements

All EPR experiments were conducted at X band microwave frequency (ca. 9.5 GHz). The CW EPR spectra recorded at 120 K were collected on a Bruker EMX spectrometer equipped with an ER4119-SHQE resonator operating at 100 kHz field modulation frequency, 0.5 mT field modulation amplitude, 5.12 ms time constant, 10.24 ms conversion time,  $1 \times 10^4$  receiver gain and 2 mW of microwave power. The CW EPR spectra recorded at 5 K were collected on a Bruker Elexsys E500 spectrometer equipped with an ER4119-SHQE resonator operating at 100 kHz field modulation frequency, 0.5 mT field modulation amplitude, 3 points of manual moving average filter, 40 dB receiver gain and 2 mW of microwave power.

All pulse EPR measurements were carried out on a Bruker Elexsys E580 system equipped with a Bruker EN4118X-MD4 resonator operating at 5 K. Additional field swept echo detected EPR spectra were recorded utilising a primary Hahn echo pulse sequence  $\pi/2-\tau-\pi-\tau$ -echo with  $\pi=32$  ns and  $\tau=400$  ns. Echo integration was performed using 4059  $\mu$ s shot repetition time, 50 shots per point and at 6.32 mW of microwave power. Hahn echo decay experiments were carried out at 178.3 mT by increasing the inter-pulse delay,  $\tau$ , of the primary echo sequence  $\pi/2-\tau-\pi-\tau$ -echo, using the same shot repetition time, shots per point and microwave power. Subsequently, microwave pulse lengths of  $\pi=208$  ns were used to suppress the proton-electron spin modulation. The phase memory time  $T_M$  (or spin-spin relaxation time constant,  $T_2$ ) was estimated from fitting the normalised spin-echo area with the following stretched exponential functions, where  $T_M$  is the phase memory time and  $s$  the stretching parameter equation (1):

$$A_N(2\tau) = A_0 e^{-\left(\frac{2\tau}{T_M}\right)^s}$$

The inversion recovery pulse sequence, *inversion pulse*-  $T-\pi/2-\tau-\pi-\tau$ -echo, was recorded with  $\pi=32$  ns,  $\tau=200$  ns and variable  $T$ , again keeping the same shot repetition time, shots per point and microwave power. The spin-lattice relaxation time constant,  $T_1$ , was estimated by fitting the normalised recovered spin-echo area with the following exponential function, where  $A_0$  and  $A_1$  are amplitudes, equation (2):

$$A_N(t) = A_0 + A_1 \left(1 - e^{-\frac{t}{T_1}}\right)$$

All CW EPR spectra were simulated using the EasySpin<sup>[63]</sup> Matlab toolbox.

## DFT Calculations

Spin unrestricted Density Functional Theory (DFT) geometry optimisations were performed using the Gaussian 09 computational chemistry software package.<sup>[64]</sup> All optimisations were performed using the B3LYP<sup>[65]</sup> exchange-correlation functional alongside Grimme's D3<sup>[66]</sup> dispersion correction at tight Self Consistent Field (SCF) and geometry tolerances. The Pople basis set 6-311+G(2d,p)<sup>[67]</sup> was applied to all C, H, O and N atoms, as well as the Ahlrich basis set def2-TZVPP<sup>[68]</sup> applied to the Co centre. Ground state geometries for a given complex, as well as  $\Delta E$ , did not differ significantly when optimised with and without an implicit solvent. Thus, an implicit solvent was not applied in this work due to the added computational expense which lacked any accuracy improve-

ments. This protocol was used for the structures where  $S=1/2$  in the LS case and  $S=3/2$  in the HS case. The energies of both LS and HS states with and without the coordination of the pyridyl bases were evaluated at the same level of theory as above, along with computation of natural bonding orbitals (NBO's) to determine the electronic orbital ground states of all LS complexes and the atomic charge on the Co centre in both LS and HS states.

The optimized LS structures were then subjected to spectroscopic calculations (Spin Hamiltonian Parameter / SHP calculations), performed with the ORCA package.<sup>[69]</sup> For the computation of  $g$  and  $A$  tensors for the LS optimised complexes, we employed the same approach used in the works of Vinck *et al.*,<sup>[36]</sup> which proved suitable in the investigation of [Co(1)] bearing weakly coordinated organic acids. Specifically, EPR-III<sup>[70]</sup> applied to nitrogen atoms, "CoreProp" (CP(PPP)) for the cobalt centre and def2-TZVPP on all other atoms with the B3LYP exchange-correlation functional. Relativistic effects were included in calculation of SHP's via a mean-field approximation to spin-orbit coupling (SOMF keyword). These are known not to be crucial for first-row TMs, but were included to ensure calculated SHPs provided as accurate as possible starting point for further simulation. DFT is limited in accuracy when computing SHP's for Co(II) complexes and the well documented limitations of these methods are discussed in the ESI.

## Acknowledgements

The authors thank Dr. Jamie Platts (Cardiff University) for advice with the DFT calculations, Dr. Emma Richards (Cardiff University) for advice with the EPR measurements and EPSRC for funding (EP/R04483X).

## Conflict of Interest

The authors declare no conflict of interest.

## Data Availability Statement

The data that support the findings of this study are available on the Cardiff University Research Portal ([https://research.cardiff.ac.uk/converis/portal/overview?lang=en\\_GB](https://research.cardiff.ac.uk/converis/portal/overview?lang=en_GB)) or from the corresponding authors upon reasonable request.

**Keywords:** Cobalt · Density functional calculations · EPR · Spin crossover · Spin distribution

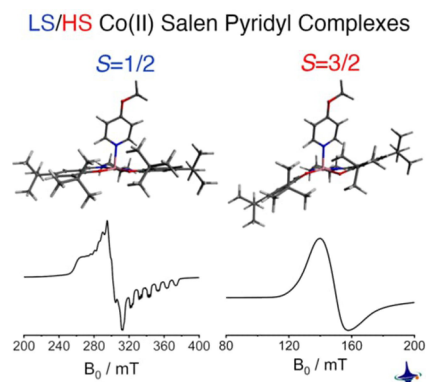
- [1] H. J. Shepherd, G. Molnár, W. Nicolazzi, L. Salmon, A. Bousseksou, *Eur. J. Inorg. Chem.* **2012**, *2013*, 653–661.
- [2] T. Jurca, A. Farghal, P. H. Lin, I. Korobkov, M. Murugesu, D. S. Richeson, *J. Am. Chem. Soc.* **2011**, *133*, 15814–15817.
- [3] G. Molnár, L. Salmon, W. Nicolazzi, F. Terki, A. Bousseksou, *J. Mater. Chem. C* **2014**, *2*, 1360–1366.
- [4] A. Gee, A. H. Jaafar, B. Brachňáková, J. Massey, C. H. Marrows, I. Šalitroš, N. T. Kemp, *J. Phys. Chem. C* **2020**, *124*, 13393–13399.
- [5] O. Kahn, C. J. Martinez, *Science* **1998**, *279*, 44–48.
- [6] L. Váhovská, S. Vitushkina, I. Potočňák, Z. Trávníček, R. Herchel, *Dalton Trans.* **2018**, *47*, 1498–1512.
- [7] L. Cambi, L. Szegő, *Ber. Dtsch.* **1933**, *66*, 656–661.

- [8] M. Nihei, T. Shiga, Y. Maeda, H. Oshio, *Coord. Chem. Rev.* **2007**, *251*, 2606–2621.
- [9] K. Senthil Kumar, Y. Bayeh, T. Gebretsadik, F. Elemo, M. Gebrezgiabher, M. Thomas, M. Ruben, *Dalton Trans.* **2019**, *48*, 15321–15337.
- [10] R. G. Miller, S. Narayanaswamy, S. M. Clark, P. Dera, G. B. Jameson, J. L. Tallon, S. Brooker, *Dalton Trans.* **2015**, *44*, 20843–20849.
- [11] M. C. Young, E. Liew, J. Ashby, K. E. Mc Coy, R. J. Hooley, *Chem. Commun.* **2013**, *49*, 6331–6333.
- [12] C. Lochenie, J. Heinz, W. Milius, B. Weber, *Dalton Trans.* **2015**, *44*, 18065–18077.
- [13] S. Schönfeld, K. Dankhoff, D. Baabe, M. K. Zaretske, M. Bröring, K. Schötz, A. Köhler, G. Hörner, B. Weber, *Inorg. Chem.* **2020**, *59*, 8320–8333.
- [14] D. H. Ren, X. L. Sun, L. Gu, D. Qiu, Z. Li, Z. G. Gu, *Inorg. Chem. Commun.* **2015**, *51*, 50–54.
- [15] I. Nemeč, R. Herchel, R. Boča, Z. Trávníček, I. Svoboda, H. Fuess, W. Linert, *Dalton Trans.* **2011**, *40*, 10090–10099.
- [16] N. P. Van Leest, W. Stroek, M. A. Siegler, J. Ivar van der Vlugt, B. de Bruin, *Inorg. Chem.* **2020**, *59*, 12903–12912.
- [17] Y. Guo, X. L. Yang, R. J. Wei, L. S. Zheng, J. Tao, *Inorg. Chem.* **2015**, *54*, 7670–7672.
- [18] R. A. Taylor, A. J. Lough, M. T. Lemaire, *J. Mater. Chem. C* **2016**, *4*, 455–459.
- [19] A. Pezeshk, F. T. Greenaway, J. C. Dabrowiak, G. Vincow, *Inorg. Chem.* **1978**, *17*, 1717–1724.
- [20] S. Hayami, Y. Komatsu, T. Shimizu, H. Kamihata, Y. H. Lee, *Coord. Chem. Rev.* **2011**, *255*, 1981–1990.
- [21] S. Kremer, W. Henke, D. Reinen, S. Kremer, W. Henke, D. Reinen, *Inorg. Chem.* **1982**, *21*, 3013–3022.
- [22] J. Zhao, Q. Peng, Z. Wang, W. Xu, H. Xiao, Q. Wu, H. L. Sun, F. Ma, J. Zhao, C. J. Sun, J. Zhao, J. Li, *Nat. Commun.* **2019**, *10*, 1–8.
- [23] I. Krivokapic, M. Zerara, M. L. Daku, A. Vargas, C. Enachescu, C. Ambrus, P. Tregenna-Piggott, N. Amstutz, E. Krausz, A. Hauser, *Coord. Chem. Rev.* **2007**, *251*, 364–378.
- [24] H. A. Goodwin, in *Top. Curr. Chem.* (Eds.: P. Gütllich, H. A. Goodwin), Springer, Berlin, Heidelberg, **2004**, pp. 23–47.
- [25] J. Zarembowitch, O. Kahn, *Inorg. Chem.* **1984**, *23*, 589–593.
- [26] B. J. Kennedy, G. D. Fallon, B. M. K. C. Gatehouse, K. S. Murray, *Inorg. Chem.* **1984**, *23*, 580–588.
- [27] P. Thuéry, J. Zarembowitch, *Inorg. Chem.* **1986**, *25*, 2001–2008.
- [28] Z. Wen, L. Zhou, J. F. Cheng, S. J. Li, W. L. You, X. Wang, *J. Phys. Condens. Matter* **2018**, *30*, 1–7.
- [29] P. Charpin, M. Nierlich, D. Vigner, M. Lance, P. Thuery, J. Zarembowitch, F. D'ivoire, *J. Crystallogr. Spectrosc. Res.* **1988**, *18*, 429–437.
- [30] A. Kochem, H. Kanso, B. Baptiste, H. Arora, C. Philouze, O. Jarjayes, H. Vezin, D. Luneau, M. Orio, F. Thomas, *Inorg. Chem.* **2012**, *51*, 10557–10571.
- [31] J. Palion-Gazda, B. Machura, R. Kruszynski, T. Granca, F. Lloret, M. Julve, *Inorg. Chem.* **2017**, *56*, 45.
- [32] J. Palion-Gazda, A. Świtlicka-Olszewska, B. Machura, T. Granca, E. Pardo, F. Lloret, M. Julve, *Inorg. Chem.* **2014**, *53*, 10009–10011.
- [33] S. Ghosh, S. Selvamani, S. Mehta, A. Mondal, *Dalton Trans.* **2020**, *49*, 9208–9212.
- [34] V. Nikhil Raj, M. K. Bhar, T. A. Khan, S. Jain, F. Perdih, P. Mitra, A. K. Sharma, *MRS Adv.* **2017**, *357*, 1–8.
- [35] A. G. Starikov, V. I. Minkin, A. A. Starikova, *J. Struct. Chem.* **2014**, *25*, 1865–1871.
- [36] E. Vinck, E. Carter, D. M. Murphy, S. Van Doorslaer, *Inorg. Chem.* **2012**, *51*, 8014–8024.
- [37] G. Dupouy, M. Marchivie, S. Triki, J. Sala-Pala, C. J. Gómez-García, S. Pillet, C. Lecomte, J. F. Létard, *Chem. Commun.* **2009**, *47*, 3404–3406.
- [38] A. Hauser, C. Enachescu, M. L. Daku, A. Vargas, N. Amstutz, *Coord. Chem. Rev.* **2006**, *250*, 1642–1652.
- [39] M. A. Hitchman, *Inorg. Chem.* **1982**, *1745*, 821–823.
- [40] C. Daul, C. W. Schläpfer, A. von Zelewsky, *Struct. Bond.* **1979**, *36*, 129–171.
- [41] A. Huber, L. Müller, H. Elias, R. Klement, M. Valko, *Eur. J. Inorg. Chem.* **2005**, 1459–1467.
- [42] E. Vinck, D. M. Murphy, I. A. Fallis, R. R. Strevens, S. Van Doorslaer, *Inorg. Chem.* **2010**, *49*, 2083–2092.
- [43] M. Baumgarten, C. J. Winscom, W. Lubitz, *Appl. Magn. Reson.* **2001**, *20*, 35–70.
- [44] E. Vinck, S. Van Doorslaer, D. M. Murphy, I. A. Fallis, *Chem. Phys. Lett.* **2008**, *464*, 31–37.
- [45] M. A. Hitchman, *Inorg. Chem.* **1977**, *16*, 1985–1993.
- [46] F. Neese, *J. Chem. Phys.* **2001**, *115*, 11080–11096.
- [47] S. Thies, C. Bornholdt, F. Köhler, F. D. Sönnichsen, C. Näther, F. Tuczec, R. Herges, *Chem. Eur. J.* **2010**, *16*, 10074–10083.
- [48] H. Kurz, K. Schötz, I. Papadopoulos, F. W. Heinemann, H. Maid, D. M. Guldi, A. Köhler, G. Hörner, B. Weber, *J. Am. Chem. Soc.* **2021**, *143*, 3466–3480.
- [49] A. V. Shokurov, D. S. Kutsybala, A. P. Kroitor, A. A. Dmitrienko, A. G. Martynov, Y. Y. Enakieva, A. Y. Tsvadze, S. L. Selektor, Y. G. Gorbunova, *Molecules* **2021**, *26*, 1–13.
- [50] C. W. Anson, S. Ghosh, S. Hammes-Schiffer, S. S. Stahl, *J. Am. Chem. Soc.* **2016**, *138*, 4186–4193.
- [51] E. Jorin, A. Schweiger, H. H. Gunthard, *Chem. Phys. Lett.* **1980**, *69*, 193–197.
- [52] L. Chiang, L. E. N. Allan, J. Alcantara, M. C. P. Wang, T. Storr, M. P. Shaver, *Dalton Trans.* **2014**, *43*, 4295–4304.
- [53] N. Bresciani, L. Randaccio, *J. Chem. Soc. Dalton Trans.* **1974**, 1606–1609.
- [54] N. Bresciani, M. Calligaris, G. Nardin, L. Randaccio, *J. Chem. Soc. Dalton Trans.* **1974**, 498–502.
- [55] M. A. Hitchman, *Inorg. Chim. Acta* **1978**, *26*, 237–245.
- [56] P. C. Kang, G. R. Eaton, S. S. Eaton, *Inorg. Chem.* **1994**, *33*, 3660–3665.
- [57] F. A. Walker, in *Handb. Porphy. Sci.* (Eds.: K. M. Kadish, K. M. Smith, R. Guilard), World Scientific, Hackensack NJ, **2010**, pp. 1–337.
- [58] L. G. Marzilli, P. A. Marzilli, *Inorg. Chem.* **1972**, *11*, 457–461.
- [59] S. A. Cantalupo, S. R. Fiedler, M. P. Shores, A. L. Rheingold, L. H. Doerrer, *Angew. Chem. Int. Ed.* **2012**, *51*, 1000–1005; *Angew. Chem.* **2012**, *124*, 1024–1029.
- [60] P. N. Dwyer, P. Madura, W. R. Scheidt, *J. Am. Chem. Soc.* **1974**, *96*, 4815–4819.
- [61] S. Ye, F. Neese, *Inorg. Chem.* **2010**, *49*, 772–774.
- [62] B. J. Kennedy, K. S. Murray, *Inorg. Chim. Acta* **1987**, *134*, 249–254.
- [63] S. Stoll, A. Schweiger, *J. Magn. Reson.* **2006**, *178*, 42–55.
- [64] M. J. Frisch, G. Trucks, H. Schlegel, G. Scuseria, M. Robb, J. Cheeseman, G. Scalmani, V. Barone, B. Mennucci, G. Petersson, H. Nakatsuji, M. Caricato, X. Li, H. Hratchian, A. Izmaylov, J. Bloino, G. Zheng, J. Sonnenberg, M. Hada, M. Ehara, K. Toyota, R. Fukuda, J. Hasegawa, M. Ishida, T. Nakajima, Y. Honda, O. Kitao, H. Nakai, T. Vreven, J. Montgomery, J. Peralta, F. Ogliaro, M. Bearpark, J. Heyd, E. Brothers, K. Kudin, V. Staroverov, R. Kobayashi, J. Normand, K. Raghavachari, P. Rendell, J. Burant, S. Iyengar, J. Tomasi, M. Cossi, N. Rega, J. Millam, M. Klene, J. Knox, J. Cross, V. Bakken, C. Adamo, J. Jaramillo, R. Gomperts, R. Stratmann, O. Yazyev, A. Austin, R. Cammi, C. Pomelli, J. Ochterski, R. Martin, K. Morokuma, V. Zakrzewski, G. Voth, P. Salvador, J. Dannenberg, S. Dapprich, A. Daniels, O. Farkas, J. Foresman, J. Ortiz, J. Cioslowski, D. Fox, *Gaussian 09, Revision D.01*, Gaussian, Inc.: Wallingford, CT, **2014**.
- [65] F. J. Devlin, J. W. Finley, P. J. Stephens, M. J. Frisch, *J. Phys. Chem. C* **1995**, *99*, 16883–16902.
- [66] S. Grimme, J. Antony, S. Ehrlich, H. Krieg, *J. Chem. Phys.* **2010**, *132*, 154104–154104–19.
- [67] R. Krishnan, J. S. Binkley, R. Seeger, J. A. Pople, *J. Chem. Phys.* **1980**, *72*, 650–654.
- [68] R. J. Schäfer, A. Horn, H. Ahlrichs, *J. Chem. Phys.* **1992**, *97*, 2571–2577.
- [69] F. Neese, The ORCA Program, *Wiley Interdiscip. Rev.: Comput. Mol. Sci.* **2012**, *2*, 73–78.
- [70] V. Barone, D. P. Chong, *Recent Advances in Density Functional Methods*, World Scientific, Singapore, **1996**.

Manuscript received: December 13, 2021  
Revised manuscript received: February 1, 2022

## RESEARCH ARTICLE

This graphical abstract shows the substrate mediate spin distribution of a Co(II) salen-type complex is studied via EPR and DFT. The rationale of pKa-H, sterics and relaxation times are all important in understanding the distribution of spin-states.



G. Magri\*, Dr. A. Folli, Prof. D. M. Murphy\*

1 – 11

**Monitoring the Substrate-Induced Spin-State Distribution in a Cobalt(II)-Salen Complex by EPR and DFT**

